Experimental Observation of Bethe Strings

Zhe Wang[1,2], Jianda Wu[3], Wang Yang[3], Anup Kumar Bera[4,5], Dmytro Kamenskyi[6], A.T.M. Nazmul Islam[4], Shenglong Xu[3], Joseph Matthew Law[7], Bella Lake[4,8], Congjun Wu[3], Alois Loidl[1]

[1]Experimental Physics V, Center for Electronic Correlations and Magnetism, Institute of Physics, University of Augsburg, 86135 Augsburg, Germany
[2]Institute of Radiation Physics, Helmholtz-Zentrum Dresden-Rossendorf, 01328 Dresden, Germany
[3]Department of Physics, University of California, San Diego, California 92093, USA
[4]Helmholtz-Zentrum Berlin für Materialien und Energie, 14109 Berlin, Germany
[5]Solid State Physics Division, Bhabha Atomic Research Centre, Mumbai 400085, India
[6]High Field Magnet Laboratory, Radboud University, 6525 ED Nijmegen, The Netherlands
[7]Hochfeld Magnetlab Dresden, Helmholtz-Zentrum Dresden-Rossendorf, 01314 Dresden, Germany
[8]Institut für Festkörperphysik, Technische Universität Berlin, 10623 Berlin, Germany

Dated: 18th September 2017

Almost one century ago, string states - complex bound states (Wellenkomplexe) of magnetic excitations - have been predicted to exist in one-dimensional quantum magnets[1] and since then become a subject of intensive theoretical studies[2,3,4,5,6,7,8,9,10,11]. However, experimental realization and identification of string states in a condensed-matter system remain an unsolved challenge up to date. Here we use high-resolution terahertz spectroscopy to resolve string states in the antiferromagnetic Heisenberg-Ising chain $SrCo_2V_2O_8$ in strong longitudinal magnetic fields. In the field-induced quantum critical regime, we identify strings and fractional magnetic excitations, which are precisely described by the Bethe ansatz. Close to the quantum criticality, the string excitations govern the quantum spin dynamics, while the fractional excitations, dominant at low energies, reflect the antiferromagnetic quantum fluctuations.

In a ferromagnet, magnons are the elementary quasiparticle excitations above the ground state and govern the low-temperature thermodynamics[4]. For the excited states with two or more magnons, a description in terms of free quasiparticles is very incomplete, especially in one and two dimensions, because due to the exchange interactions the magnons can form bound states sharing common center-of-mass momenta[12]. For a one-dimensional (1D) system, the magnon bound states can be viewed as magnetic solitons[13] in the classical limit, which correspond to strings of flipped spins that exist as bound entities in the chain. The study of dynamical properties of the interacting magnetic excitations is not only of interest for potential applications in quantum information[14], but also provides enlightening insight into fundamental aspects of quantum magnetism as well as quantum many-body systems[15].

In the 1D spin-1/2 Heisenberg model, a paradigmatic model of interacting spin systems, the existence of bound states was predicted for the first time early in 1930s by Bethe for two magnons[1]. The systematic ansatz introduced by Bethe for exactly calculating the eigenvalues and eigenstates of the Heisenberg model was later generalized for the description of multi-magnon bound states, the so-called strings[3], also in models beyond the isotropic limit[4,6,8,9]. It was generally believed that the spin dynamics is governed by low-energy multi-particle excitations[7,16,17,18,19], till recently the excitations of two-magnon bound states (2-string states) were theoretically suggested to be dominant in the isotropic Heisenberg antiferromagnet[10]. However, the string excitations are sensitive to exchange anisotropy: For an easy-plane anisotropy, although the spin excitations remain gapless, the dynamical response of string states is significantly smaller compared with the fractional multi-particle excitations (spinons)[8,9]. Also in the spin-gapped Heisenberg-Ising antiferromagnet with easy-axis anisotropy, the dynamical properties are dominated by the fractional spinon excitations[19,20]. Hence, an experimental realization of the string states is a very difficult challenge and so far remains unsolved in condensed-matter systems. Here, by performing terahertz spectroscopy on the 1D Heisenberg-Ising antiferromagnetic system $SrCo_2V_2O_8$ in the longitudinal magnetic fields, we show that when the spin gap is closed above a field-induced quantum phase transition at $B_c = 4$ T, 2-string and 3-string states are identified in the quantum critical regime, before a fully field-polarized state is reached at $B_s = 28.7$ T. On decreasing magnetic field from B_s, the dominant role of the low-energy fractional multi-particles in the dynamical response is gradually taken over by the string states which finally govern the quantum spin dynamics close to the quantum phase transition.

The realization of the 1D Heisenberg-Ising model in $SrCo_2V_2O_8$ is based on its crystal structure and the dominant nearest-neighbour antiferromagnetic interactions (Fig. 1a). The screw chains of CoO_4 octahedra with fourfold screw axis running along the crystallographic c direction are arranged in a tetragonal structure. Due to spin-orbit coupling, the atomic magnetic moments of the Co^{2+} ions, comprising the spin and orbital degrees of freedom, are exposed to an Ising anisotropy. The crystal-electric field in the CoO_4 octahedra lifts the twelvefold degeneracy of the Co^{2+} moments, resulting in a Kramers-doublet ground state with the total angular momentum 1/2 (Ref. 21). Magnetization and neutron diffraction experiments reveal that the Ising anisotropy forces the atomic magnetic moments along the c axis, with a Néel-type collinear antiferromagnetic order stabilized below $T_N = 5$ K (Ref. 22).

Superexchange interactions between the magnetic moments in the chains of $SrCo_2V_2O_8$ are described by the Hamiltonian of the 1D spin-1/2 Heisenberg-Ising model[23,24],

$$H = J \sum_{n=1}^{N} \left[\left(S_n^x S_{n+1}^x + S_n^y S_{n+1}^y \right) + \Delta S_n^z S_{n+1}^z \right] - g_\parallel \mu_B B \sum_{n=1}^{N} S_n^z \qquad (1)$$

where $J > 0$ is the antiferromagnetic coupling between neighboring spins and $\Delta > 1$ takes the Ising anisotropy between the longitudinal and transverse spin couplings into account. The last term includes the Zeeman interaction in a longitudinal magnetic field B along the c axis with the g-factor $g_\parallel$ and the Bohr magneton μ_B.

The Néel ground state at zero field can be illustrated by an antiparallel alignment of neighboring spins, corresponding to the total spin-z quantum number $S_T^z = 0$ (Fig. 1a). One spin-flip creates an excitation of two spinons[20] that can separately propagate along the chain by subsequent spin-flips. In momentum space they form a two-particle excitation continuum[16,17,18,19] that is gapped above the antiferromagnetic ground state.

Via the Zeeman interaction a longitudinal magnetic field can reduce and finally close the spin gap at a critical field B_c (Ref. 2). Before reaching the fully polarized state ($B > B_s$, Fig.1a) where the elementary excitations are gapped magnons, the system enters a gapless phase corresponding to the critical regime ($B_c < B < B_s$). In this regime, a general ground state with an arbitrary value of S_T^z is illustrated in Fig. 1b, and fundamentally new and exotic states can be excited by flipping a single spin (Figs. 1c to 1f). According to the Bethe ansatz[1], the spin excitations in the critical regime can be bound states of n magnons (n-string states)[3,4], or low-energy spinon-like quasiparticles[5,7,8,9,10]. The spinon-like quasiparticles, which also form multi-particle continua[25] like spinons (see Methods), were named psinons/antipsinons[7,8] in the context of Bethe ansatz, to distinguish from the spinons in zero field. This nomenclature will be adopted in the following, because, more importantly, our results reveal that the excitations of psinon-psinons or psinon-antipsinons obey the opposite selection rules (Figs. 1c and 1d).

Since excitations with $\Delta S_T^z = +1$ or -1 are allowed by selection rules that govern the interaction with the magnetic field of photons or with the magnetic moment of neutrons, the excited states illustrated in Figs. 1c to 1f should be observable by optical or neutron scattering experiments. Here, we report terahertz optical spectroscopy on the Heisenberg-Ising antiferromagnetic chain SrCo$_2$V$_2$O$_8$ in a longitudinal magnetic field up to 30 T. Our study provides clear experimental evidence for the existence of the 2-string and 3-string states, as well as the fractional multi-particle excitations, characterizing the quantum spin dynamics of the one-dimensional spin-1/2 Heisenberg-Ising model.

In a longitudinal magnetic field, S_T^z is a good quantum number. Hence, the eigenstates of the Heisenberg-Ising model can be accordingly classified, and described by a general Bethe-ansatz wavefunction

$$|\varphi\rangle = \sum_{1 \leq n_1 \leq \cdots \leq n_r \leq N} a(n_1, n_2, \ldots, n_r) |n_1, n_2, \ldots, n_r\rangle$$

for a total spin-z quantum number $S_T^z = N/2 - r$ (Fig. 1b), with N denoting the length of the chain, and r flipped spins at the sites of $n_1, n_2, \ldots,$ and n_r in the chain with respect to the fully spin-polarized state $|\ldots \rightarrow\rightarrow\rightarrow \cdots\rangle$, i.e. $|n_1, n_2, \ldots, n_r\rangle = S_{n_1}^- S_{n_2}^- \ldots S_{n_r}^- |\ldots \rightarrow\rightarrow\rightarrow \cdots\rangle$ where $S_{n_j}^\pm \equiv S_{n_j}^x \pm i S_{n_j}^y$ is the operator flipping the spin of site n_j. We use the Bethe ansatz to obtain the coefficients $a(n_1, n_2, \ldots, n_r)$ and eigenenergies of the ground state as well as excited states for every S_T^z sector (see Methods). Corresponding to the real and complex momenta in the solutions of the Bethe-ansatz equations[1,3,4,6,8,9,10,11], the excited states of psinon-(anti)psinons and n-strings are labelled as R_q and $\chi_q^{(n)}$, respectively, with the subscript indexing the corresponding transfer momenta. Those excitations allowed in optical experiments obey the selection rule $\Delta S_T^z = +1$ or -1, which contribute to the dynamic structure factor $S^{-+}(q, \omega)$ or $S^{+-}(q, \omega)$, respectively. The two quantities are defined by $S^{a\bar{a}}(q, \omega) = \pi \sum_\mu |\langle \mu | S_q^{\bar{a}} | G \rangle|^2 \delta(\omega - E_\mu + E_G)$ in which $S_q^\pm = \frac{1}{\sqrt{N}} \sum_n e^{iqn} S_n^\pm$ and $\bar{a} = -a$ with $a = +$ or $-$, and $|G\rangle$ and $|\mu\rangle$ are the ground state and the excited state with eigenenergies of E_G and E_μ, respectively. Hence, we can quantitatively single out contributions of string excitations, as well as of psinon-(anti)psinon pairs, to the relevant dynamic structure factors. The string excitations with higher energies and characteristic field dependencies can be well distinguished from the low-energy psinon-(anti)psinon pairs (see

Methods). This enables us to precisely compare to the experimental results as a function of the longitudinal field and to identify the nature of each observed mode.

Figure 2a shows transmission spectra at various frequencies below 1 THz as a function of longitudinal magnetic fields. At 0.195 THz, two transmission minima can be observed at 2.41T (mode $1-$) and 6.18 T (mode R_0), below and above the critical field $B_c = 4$ T, respectively. With increasing magnetic fields, mode $1-$ shifts to lower, and mode R_0 to higher frequencies. The mode $1-$ together with the modes $1+$, $2-$, $2+$, and $3-$ observed at higher frequencies (0.39 and 0.59 THz) are known as confined spinon excitations[23] due to the inter-chain couplings in the gapped Néel-ordered phase ($B < B_c$). Well below the critical field (Fig. 2b), the confined spinons exhibit Zeeman splitting with linear field dependence[23]. Close to the critical field B_c, the mode $1-$ softens, concomitant with a significant hardening of the mode $1+$. This indicates that the inter-chain couplings are suppressed above B_c, and the system enters the field-induced critical regime of one dimension. Completely different excitation spectra appear in the critical regime: In the same frequency range (Fig. 2a), we unambiguously observe three sharp modes as denoted by R_0, $\chi_0^{(2)}$, and $\chi_\pi^{(2)}$. With increasing magnetic field well above the critical field, the eigenenergies of the three modes increase linearly with different slopes (Fig. 2b).

Using magneto-optic spectroscopy in a high-field laboratory, we are able to extend the search for magnetic excitations to a much larger spectral range and to higher magnetic fields up to 30 T, covering the complete critical regime ($B_c < B < B_s$) and the field-polarized ferromagnetic phase ($B > B_s = 28.7$ T). As displayed in Fig. 3, the magnetic excitations are represented by the peaks in the absorption-coefficient spectra at various magnetic fields. At 10 T we not only identify the modes R_0, $\chi_0^{(2)}$, and $\chi_\pi^{(2)}$ at 1.66, 3.67, and 4.23 meV, respectively, in a sequence of increasing energies, but also a higher-energy mode $R_{\pi/2}$ at 5.82 meV. While the modes R_0 and $\chi_\pi^{(2)}$ have comparable absorption coefficients, the mode $\chi_0^{(2)}$ is much weaker, which is consistent with the low-field measurements (e.g. the 0.59 THz spectrum in Fig. 2a). In higher magnetic fields, the mode $R_{\pi/2}$ softens, while the other modes R_0, $\chi_0^{(2)}$, and $\chi_\pi^{(2)}$ shift to higher energies. Above the low-energy phonon bands (see Methods), we resolve a further high-energy magnetic excitation $\chi_{\pi/2}^{(3)}$ of 14.6 meV at 13 T, which shifts to higher energies with increasing magnetic field (Fig. 3b). The field dependence of the eigenfrequencies of the five observed modes R_0, $R_{\pi/2}$, $\chi_0^{(2)}$, and $\chi_\pi^{(2)}$, and $\chi_{\pi/2}^{(3)}$ is summarized in Fig. 4 (symbols). The field dependencies are linear for all the modes, each with distinct slope and characteristic energy.

From the Bethe-ansatz calculations[6], we can single out various excitations and evaluate their respective contributions to the dynamic structure factors $S^{+-}(q, \omega)$ and $S^{-+}(q, \omega)$ (Methods). In accord with Brillouin-zone folding due to the fourfold screw-axis symmetry of the spin chain[22,24], in Fig. 4 we show the peak frequencies in $S^{+-}(q, \omega)$ and $S^{-+}(q, \omega)$ as a function of magnetic field (solid lines) for the transfer momenta $q = 0$, $\pi/2$, and π, to compare to the THz spectroscopic results. Excellent agreement between theory and experiment is achieved for all the five distinct magnetic excitations, which allows to unambiguously identify their nature: R_0 characterizes psinon-antipsinon pairs at $q = 0$,

while $R_{\pi/2}$ are psinon-psinon pairs at $q = \pi/2$. The psinon-antipsinon excitations R_0, related to the single spin-flip operator $S^-_{q=0}$, evolve from the magnon mode M_0 in the field-polarized ferromagnetic phase, where the largest absorption is observed experimentally (Figs. 3a and 4). Most strikingly, we are able to detect and identify the 2-string states $\chi_0^{(2)}$ and $\chi_\pi^{(2)}$ at $q = 0$ and $q = \pi$, respectively, and the 3-string states $\chi_{\pi/2}^{(3)}$ for $q = \pi/2$.

The branch of psinon-psinon pairs $R_{\pi/2}$ belongs to $S^{-+}(q, \omega)$ and obeys the selection rule of $\Delta S^z_T = +1$. Hence, the psinon-psinon excitations correspond to flipping one spin into the direction of the magnetic field (Fig. 1c), which will decrease the Zeeman energy. Therefore, the mode $R_{\pi/2}$ softens with increasing field. In contrast, the psinon-antipsinon pairs and the string states, corresponding to $S^{+-}(q, \omega)$, obey the selection rule of $\Delta S^z_T = -1$ (Figs. 1d to 1f), thus their eigenenergies increase in magnetic field. The linear dependencies, essentially arising from the linear dependence of the Zeeman energy on magnetic field, are significantly renormalized due to the one-dimensional many-body interactions.

The observation of 3-string states reflects a very peculiar feature of the 1D Heisenberg-Ising model: Close to the quantum criticality even three magnons can form a stable bound state, and more surprisingly, the bound states of three magnons govern the dynamical response[26]. This is in clear contrast to the isotropic Heisenberg model, where the 2-string states dominate[10], or the models with easy-plane anisotropy, where the fractional multi-particles essentially characterize the dynamical properties[8,9]. Besides their eigenfrequencies, the contribution of the string states to the spin dynamics is also strongly field-dependent[8,9,10,26]. Starting from the quantum phase transition of the Heisenberg-Ising model[26], the increase of magnetic field leads to a decreasing contribution of the string excitations, while above the half-saturated magnetization, the low-energy multi-particle excitations become dominant and finally govern the spin dynamics when approaching the fully field-polarized limit (Methods). This is manifested by the rapidly increasing absorption of the mode R_0 (see Fig. 3).

We have identified 2-string and 3-string states in the quantum critical regime of a 1D spin-1/2 Heisenberg-Ising chain. This represents an outstanding example of experimental realization of strongly correlated quantum-states in condensed matter systems[27]. Further dynamical properties of the string states are expected from inelastic neutron-scattering study, which can probe the whole Brillouin zone also for the excitation continua[16,17,18,19,25], thus allowing a more detailed comparison to theory. The stability of the string states, indicated by our results, provides the possibility to study their non-equilibrium behavior in quantum magnets[28] as well as in the cold-atom lattice[29]. Thus, our results pave the way towards the deterministic manipulation of complex magnetic many-body states in solid-state materials, and shed light on the study of integrable quantum many-body systems in general[11,15,30].

Extended Data Figure 1 | Crystal and magnetic structure of SrCo₂V₂O₈. a, Screw chain structure is constituted by edge-shared CoO₄ octahedra. Each chain has screw-axis symmetry with a period of four Co ions (as numbered by the integers 1, 2, 3, 4 in the figure), corresponding to the lattice constant along the c axis. The Néel ordered phase is illustrated by antiparallel arrows representing magnetic moments at the Co^{2+} sites. Intra-chain nearest-neighbor interaction is denoted by J. **b,** Viewing from the c axis, each unit cell contains four screw chains with left- or right-handed screw axes, respectively. The leading inter-chain coupling $J_\perp$ is indicated, which is between the Co^{2+} ions in the same layer (denoted by the same integer number of Co site) and from chains with the same chirality. It is very small compared to the intra-chain interaction, i.e. $J_\perp/J < 10^{-2}$ (Refs. 31,32).

Extended Data Figure 2 | High-field magnetization and magnetic susceptibility of SrCo₂V₂O₈. a, Magnetization M as a function of an applied longitudinal magnetic field B along the Ising axis ($B \parallel c$) measured at 1.7 K. Theoretical magnetization of the Heisenberg-Ising chain model is shown by the dashed line. **b,** Magnetic susceptibility dM/dH as a function of the applied longitudinal field B. A quantum phase transition from the Néel-ordered phase to the critical phase is revealed by the onset of magnetization and the peak in the susceptibility curve at the critical field $B_c = 4$ T. Saturated magnetization is observed above the field $B_s = 28.7$ T and indicated by the sharp peak of the susceptibility. A small anomaly at $B_{hs} = 25$ T seen in the susceptibility is close to the field of half-saturated magnetization.

Extended Data Figure 3 | Low-energy phonon spectrum of SrCo₂V₂O₈. The phonon spectra of SrCo₂V₂O₈ measured for the polarization $E^\omega \parallel a$ at 5 K. Strong reflectivity due to phonon excitations is observed in the spectral range from 8 to 13.5 meV.

Extended Data Figure 4 | Schematic plots of patterns of Bethe quantum numbers for **a,** the ground state, **b,** one-pair psinon-psinon state $1\psi\psi$, **c,** one-pair psinon-antipsinon state $1\psi\psi^*$, and **d,** length-two string state $1\chi^{(2)}R$. The system size is taken as $N = 32$, and the magnetization is $S_T^z = 8$.

Extended Data Figure 5 | Dynamic structure factors **a,** $S^{+-}(q,\omega)$ and **b,** $S^{-+}(q,\omega)$ as functions of energy $\hbar\omega/J$ (vertical axis) and momentum q/π (horizontal axis) for $2m = 0.4$, $N = 200$. The gapless continua are formed by real Bethe eigenstates (psinon-antipsinon pairs in S^{+-} and psinon-psinon pairs in S^{-+}). For S^{+-}, the higher-energy continua correspond to excitations of 2-string ($\hbar\omega > 3J$) and 3-string ($\hbar\omega > 5J$), respectively.

Extended Data Figure 6 | The momentum integrated ratios **a,** ν_{+-} for S^{+-} and **b,** ν_{-+} for S^{-+} as functions of magnetization $2m$. In **a,** the green line is the $1\psi\psi^*$ contribution. The blue, red and the black lines are augmented by progressively taking into account the $2\psi\psi^*$, 2-string, and 3-string contributions, respectively. In **b,** the blue and black lines represent the $1\psi\psi$ and $1\psi\psi + 2\psi\psi$ contributions.

Extended Data Figure 7 | Dynamic structure factor of psinon-psinon pairs as a function of energy for $2m = 0.1$ to 0.9 at $q = 0, \pi/2$, and π.

Extended Data Figure 8 | Dynamic structure factor of psinon-antipsinon pairs as a function of energy for $2m = 0.1$ to 0.9 at $q = 0, \pi/2$, and π.

Extended Data Figure 9 | Dynamic structure factor of 2-string as a function of energy for $2m = 0.1$ to 0.9 at $q = 0, \pi/2$, and π.

Extended Data Figure 10 | Dynamic structure factor of 3-string as a function of energy for $2m = 0.1$ to 0.9 at $q = 0, \pi/2$, and π.

Author contributions Z.W. conceived and performed the optical experiments, analyzed the data, and coordinated the project under the supervision of A.L. J.W., W.Y., S.X. and C.W. carried out the Bethe-ansatz calculations. A.K.B., A.T.M.N.I. and B.L. prepared and characterized the high-quality single crystals. A.K.B. and J.M.L. performed the high-field magnetization measurements. D.K. assisted the high-field optical experiments. Z.W., J.W., W.Y., C.W. and A.L. wrote the manuscript with inputs from all authors. All authors discussed the results.

Author Information The authors declare no competing financial interests. Correspondence should be addressed to Z.W. (zhe.wang@hzdr.de).

[1] Bethe, H. Zur Theorie der Metalle. I. Eigenwerte und Eigenfunktionen der Linearen Atomkette. *Z. Phys.* **71**, 205-226 (1931).

[2] Yang, C. N. & Yang, C. P. One-Dimensional Chain of Anisotropic Spin-Spin Interactions. II. Properties of the Ground-State Energy Per Lattice Site for an Infinite System. *Phys. Rev.* **150**, 327 (1966).

[3] Gaudin, M. Thermodynamics of the Heisenberg-Ising Ring for $\Delta \geq 1$. *Phys. Rev. Lett.* **26**, 1301-1304 (1971).

[4] Takahashi, M. & Suzuki, M. One-Dimensional Anisotropic Heisenberg Model at Finite Temperatures. *Prog. Theor. Phys.* **48**, 2187-2209 (1972).

[5] Müller, G., Thomas, H., Beck, H. & Bonner, J. C. Quantum spin dynamics of the antiferromagnetic linear chain in zero and nonzero magnetic field. *Phys. Rev. B* **24**, 1429 (1981).

[6] Kitanine, N., Maillet, J. M. & Terras, V. Form factors of the XXZ Heisenberg spin-½ finite chain. *Nucl. Phys. B* **554**, 647 (1999).

[7] Karbach, M. & Müller, G. Line-shape predictions via Bethe ansatz for the one-dimensional spin-1/2 Heisenberg antiferromagnet in a magnetic field. *Phys. Rev. B* **62**, 14871-14879 (2000).

[8] Sato, J., Shiroishi, M. & Takahashi, M. Evaluation of Dynamic Spin Structure Factor for the Spin-1/2 XXZ Chain in a Magnetic Field. *J. Phys. Soc. Jpn.* **73**, 3008-3014 (2004).

[9] Caux, J.-S., Hagemans, R. & Maillet, J. M. Computation of dynamical correlation functions of Heisenberg chains: the gapless anisotropic regime. *J. Stat. Mech.* **2005**, P09003 (2005).

[10] Kohno, M. Dynamically Dominant Excitations of String Solutions in the Spin-1/2 Antiferromagnetic Heisenberg Chain in a Magnetic Field. *Phys. Rev. Lett.* **102**, 037203 (2009).

[11] Ganahl, M., Rabel, E., Essler, F. H. L. & Evertz, H. G. Observation of Complex Bound States in the Spin-1/2 Heisenberg XXZ Chain Using Local Quantum Quenches. *Phys. Rev. Lett.* **108**, 077206 (2012).

[12] Wortis, M. Bound States of Two Spin Waves in the Heisenberg Ferromagnet. *Phys. Rev.* **132**, 85-97 (1963).

[13] Fogedby, H. C. The spectrum of the continuous isotropic quantum Heisenberg chain: quantum solitons as magnon bound states. *J. Phys. C* **13**, L195-200 (1980).

[14] Subrahmanyam, V. Entanglement dynamics and quantum-state transport in spin chains. *Phys. Rev. A* **69**, 034304 (2004).

[15] Batchelor, M. T. The Bethe ansatz after 75 years. *Physics Today* **60**, 36-40 (2007).

[16] Tennant, D. A., Perring, T. G., Cowley, R. A. & Nagler, S. E. Unbound spinons in the S=1/2 antiferromagnetic chain $KCuF_3$. *Phys. Rev. Lett.* **70**, 4003-4006 (1993).

[17] Lake, B. *et al.*, Confinement of fractional quantum number particles in a condensed-matter system. *Nature Physics* **6**, 50-55 (2010).

[18] Mourigal, M. *et al.*, Fractional spinon excitations in the quantum Heisenberg antiferromagnetic chain. *Nature Physics* **9**, 435-341 (2013).

[19] Wu, L. S. *et al.*, Orbital-Exchange and Fractional Quantum Number Excitations in an f-Electron Metal, Yb_2Pt_2Pb. *Science* **352**, 1206-1210 (2016).

[20] Faddeev, L. D. & Takhtajan, L. A., What is the spin of a spin wave? *Phys. Lett. A* **85**, 375-377 (1981).

[21] Lines, M. E. Magnetic Properties of $CoCl_2$ and $NiCl_2$, *Phys. Rev.* **131**, 546 (1963).

[22] Bera, A. K., Lake, B., Stein, W.-D. & Zander S. Magnetic correlations of the quasi-one-dimensional half-integer spin-chain antiferromagnets $SrM_2V_2O_8$ (M = Co, Mn). *Phys. Rev. B* **89**, 094402 (2014).

[23] Wang, Z. *et al.*, Spinon confinement in the one-dimensional Ising-like antiferromagnet $SrCo_2V_2O_8$. *Phys. Rev. B* **91**, 140404 (2015).

[24] Wang, Z. *et al.*, From confined spinons to emergent fermions: Observation of elementary magnetic excitations in a transverse-field Ising chain. *Phys. Rev. B* **91**, 125130 (2016).

[25] Stone, M. B. *et al.*, Extended Quantum Critical Phase in a Magnetized Spin-1/2 Antiferromagnetic Chain. *Phys. Rev. Lett.* **91**, 037205 (2003).

[26] Yang, W., Wu, J., Xu, S., Wang, Z. & Wu, C. Quantum spin dynamics of the axial antiferromagnetic spin-12 XXZ chain in a longitudinal magnetic field. Preprint at https://arxiv.org/abs/1702.01854 (2017).

[27] Essler, F. H. L. & Konik, R. M. in From Fields to Strings*: Circumnavigating Theoretical Physics*, Volume 1, (World Scientific, Singapore, 2005)

[28] Nishida, Y., Kato, Y. & Batista, C. D. Efimov effect in quantum magnets. *Nature Physics* **9**, 93-97 (2013).

[29] Fukuhara, T. *et al.*, Microscopic observation of magnon bound states and their dynamics. *Nature* **502**, 76-79 (2013).

[30] Lieb, E. H. & Liniger, W. Exact Analysis of an Interacting Bose Gas. I. The General Solution and the Ground State. *Phys. Rev.* **130**, 1605 (1963).
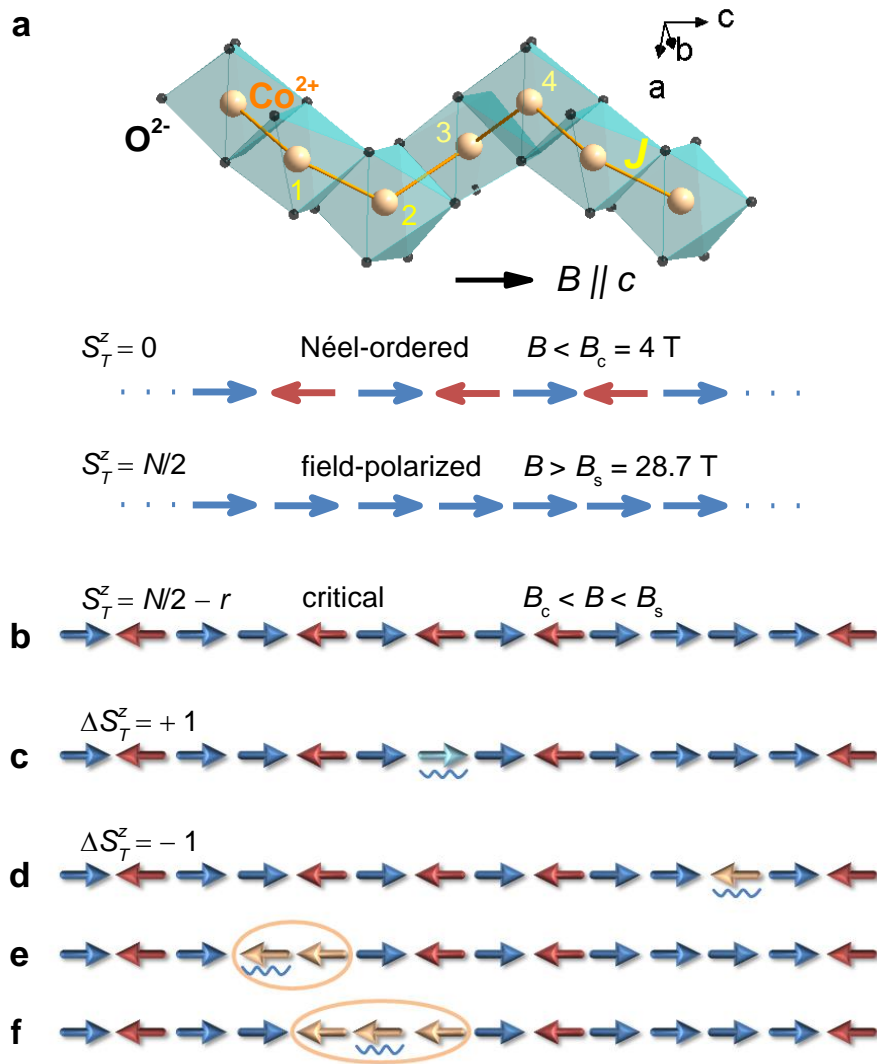
Figure 1 | Quantum spin chain in SrCo₂V₂O₈ and characteristic magnetic excitations of one dimension in the critical regime: psinon-(anti)psinons and strings.

a, Chain structure of SrCo₂V₂O₈ with a four-fold screw axis along the *c* direction: at 1.7 K Néel-ordered and field-polarized states are stabilized for longitudinal magnetic fields $B < B_c = 4$ T and $B > B_s = 28.7$ T, respectively. **b**, A representative configuration of the ground state in the critical regime ($B_c < B < B_s$) for the total spin-z quantum number $S_T^z = N/2 - r$ with r flipped spins with respect to the fully polarized state. Excitations on the ground state are allowed by the selection rule $\Delta S_T^z = +1$ for **c**, psinon-psinon, or by $\Delta S_T^z = -1$ for **d**, psinon-antipsinon, **e**, 2-string, and **f**, 3-string, that govern the interaction with the magnetic field of a photon. While the psinon-(anti)psinons can propagate throughout the chain without forming bound states, the 2-strings and 3-strings (bound states formed by two and three magnons, respectively) move as entities in the chain. The flipped spin with respect to the ground state (**b**) is indicated by a wiggly line for every excited state (**c** to **f**).
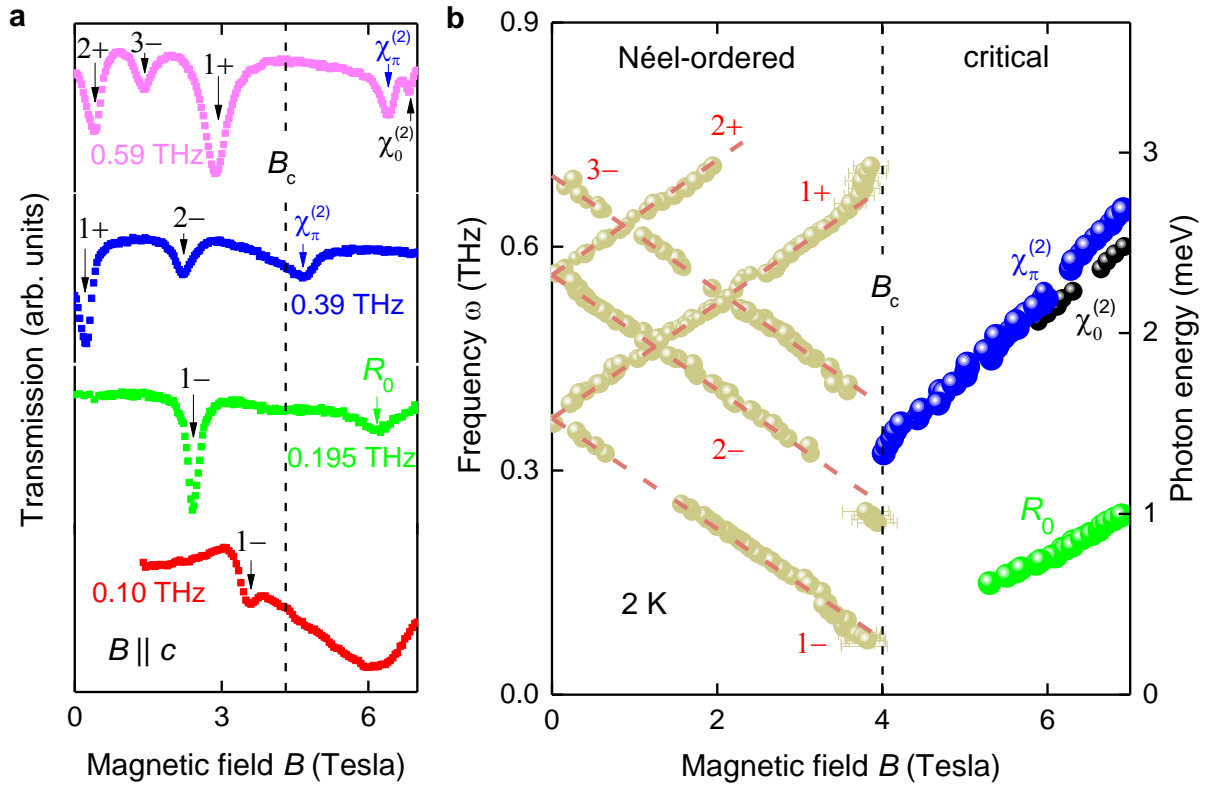
Figure 2 | Softening of spinons and emergent magnetic excitations at the quantum phase transition in SrCo₂V₂O₈.

a, Transmission spectra of magnetic excitations in $SrCo_2V_2O_8$ for various frequencies below 1 THz, measured with the applied longitudinal magnetic field $B \parallel c$ and the electromagnetic wave propagating along the c axis. Magnetic resonance excitations corresponding to transmission minima are indicated by arrows. The field-induced phase transition from the Néel-ordered phase to the critical regime is indicated by the vertical dashed line at the critical field $B_c = 4$ T.

b, Eigenfrequencies of the resonance modes as a function of the applied magnetic field. For $B < B_c$, a series of confined fractional spinon excitations split in low fields ($1\pm$, $2\pm$, etc) and follow linear field dependency. Above B_c, new modes R_0, $\chi_0^{(2)}$, and $\chi_\pi^{(2)}$ emerge with completely different field dependencies. Deviations from the linear field-dependence appear when approaching the critical field. Error bars indicate the resonance linewidths.
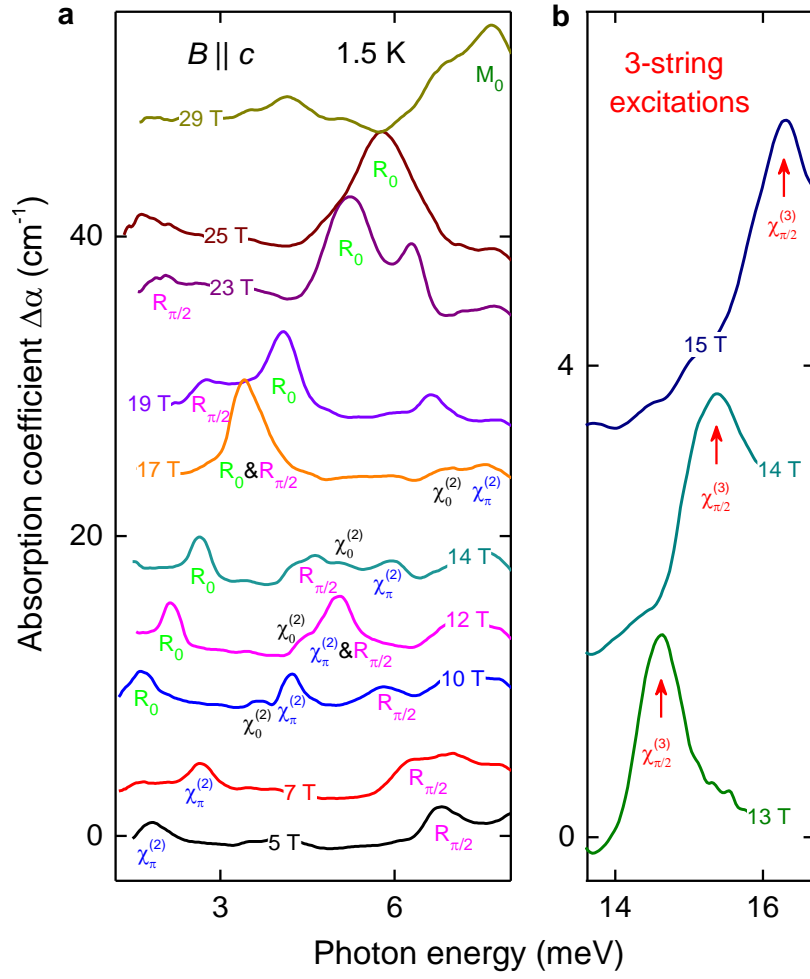
Figure 3 | Absorption spectra of psinon-psinon, psinon-antipsinon, 2-string, and 3-string excitations for $B_c < B < B_s$, and of magnons for $B > B_s$ in SrCo₂V₂O₈. Absorption spectra for various longitudinal magnetic fields in the critical regime in **a**, the low-energy and **b**, the high-energy spectral range. **a**, Four types of excitations, R_0, $R_{\pi/2}$, $\chi_0^{(2)}$, and $\chi_\pi^{(2)}$, each with a characteristic field dependence are observed in the critical regime ($B_c < B < B_s$), and the mode R_0 evolves from the mode M_0 above B_s. While the mode $R_{\pi/2}$ softens with increasing fields, eigenenergies of the other modes increase. **b**, A higher-energy mode $\chi_{\pi/2}^{(3)}$ can be resolved at relatively low magnetic fields. The spectra are shifted upwards proportional to the corresponding magnetic fields.
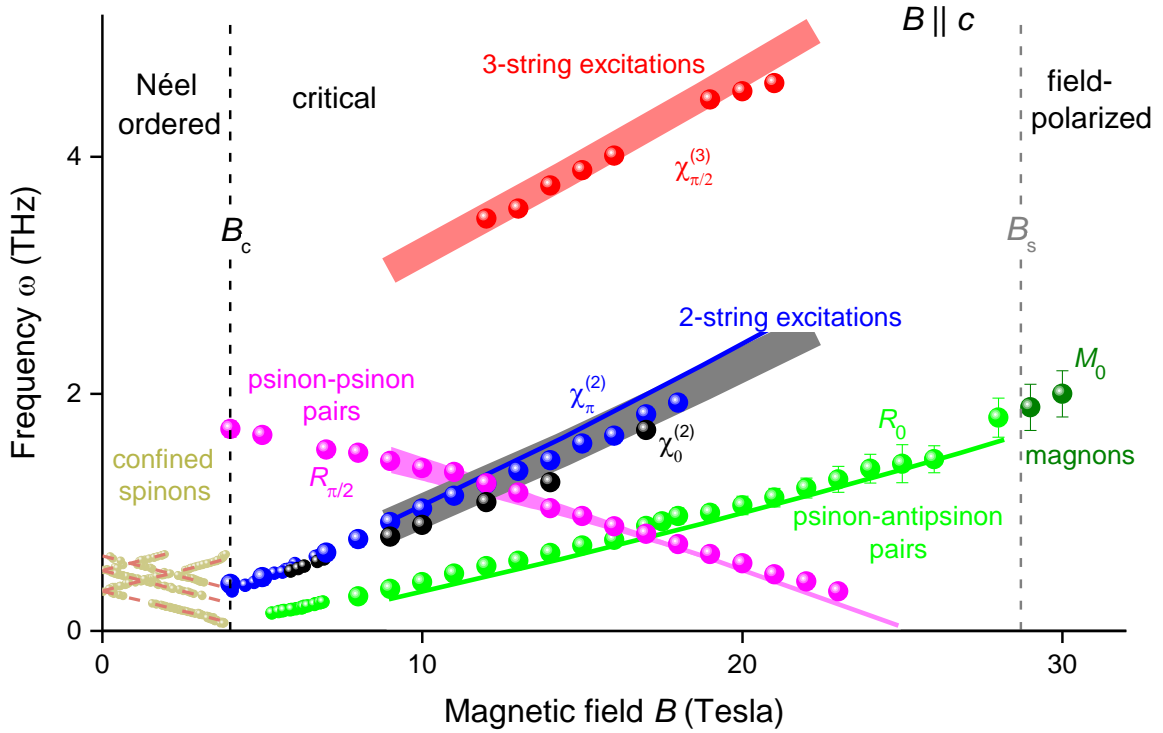
Figure 4 | Magnetic excitations in the longitudinal-field Heisenberg-Ising chain SrCo₂V₂O₈: experiment and theory.

Eigenfrequencies as a function of longitudinal magnetic field for all magnetic excitations observed experimentally are shown by symbols. Below $B_c = 4$ T confined spinons are observed in the Néel-ordered phase. In the critical regime ($B_c < B < B_s$), excitations of psinon-psinon pairs ($R_{\pi/2}$ at $q = \pi/2$), psinon-antipsinon pairs (R_0 at $q = 0$), and of complex bound states 2-strings ($\chi_\pi^{(2)}$, $\chi_0^{(2)}$ at $q = \pi, 0$) and 3-strings ($\chi_{\pi/2}^{(3)}$ at $q = \pi/2$) are identified by the field dependencies of their eigenfrequencies. Above $B_s = 28.7$ T, magnons (M_0 at $q = 0$) are observed in the field-polarized ferromagnetic phase.

Solid lines display the results of the dynamic structure factors $S^{-+}(q, \omega)$ and $S^{+-}(q, \omega)$ at $q = 0, \pi/2$, and π for the corresponding excitations of the one-dimensional spin-1/2 antiferromagnetic Heisenberg-Ising model. For all the five modes (R_0, $R_{\pi/2}$, $\chi_0^{(2)}$, and $\chi_\pi^{(2)}$, and $\chi_{\pi/2}^{(3)}$), excellent agreement between theory and experiment is achieved with the exchange interaction $J = 3.55$ meV, the g-factor $g_\parallel = 6.2$, and the Ising anisotropy $\Delta = 2$ (Ref. 24). Experimental and theoretical linewidths are indicated by error bars and shaded areas, respectively.